# 3D XFEM investigation of the plasticity effect on fatigue propagation under thermo-mechanical loading

Eric Feulvarch, Rémi Lacroix, Komlanvi Madou, Hubert Deschanels, Moïse Pignol

**Noname manuscript No.**
(will be inserted by the editor)

# 3D XFEM investigation of the plasticity effect on fatigue propagation under thermo-mechanical loading

**Eric Feulvarch · Rémi Lacroix · Komlanvi Madou · Hubert Deschanels · Moïse Pignol**

Received: date / Accepted: date

**Abstract** The aim of this paper is to propose a computation strategy for fatigue propagation simulation of a crack by taking into account the plasticity. Feulvarch *et al.* [Comput. Methods Appl. Mech. Engrg. 361 (2020) 112805] recently proposed a first XFEM formulation capable of overcoming the volumetric locking phenomenon due to plastic incompressibility in 3D. This formulation is here applied to quadratic elements for the mode I propagation of a crack in a valve structure submitted to cyclic thermo-mechanical loading. A simulation strategy is proposed where it is not necessary to compute all the cycles and thus the complete plastic history. This is of great interest because it avoids the treatment of the possible closing of the crack and uses the conventional $J$-integral. The application reveals the interest of taking plasticity into account for the propagation accuracy.

**Keywords** XFEM · Fatigue · Propagation · Plasticity · Thermo-mechanical loading

Eric Feulvarch
Univ. Lyon, ENISE, LTDS, UMR 5513 CNRS, 58 rue Jean Parot, 42023 Saint-Etienne cedex 02, France
E-mail: eric.feulvarch@enise.fr

Rémi Lacroix
ESI Group, Le Recamier, 70 rue Robert, 69458 Lyon cedex 06, France
E-mail: remi.lacroix@esi-group.com

Komlanvi Madou
ESI Group, Le Recamier, 70 rue Robert, 69458 Lyon cedex 06, France
E-mail: komlanvi.madou@esi-group.com

Hubert Deschanels
Framatome, 10 rue Juliette Recamier, 69456 Lyon cedex 06, France
E-mail: hubert.deschanels@framatome.com

Moïse Pignol
Framatome, 10 rue Juliette Recamier, 69456 Lyon cedex 06, France
E-mail: moise.pignol@framatome.com

## 1 Introduction

The eXtended Finite Element Method has been researched for many years in the field of fracture mechanics [1]. It is usually coupled with the level set functions for modeling crack geometries [2–4]. It was applied to industrial case studies [5–8] in order to study crack paths in Linear Elastic Fracture Mechanics. Extended meshfree methods [9] and isogeometric boundary element methods [10] have also been developed in the context of 3D LEFM. In elasto-plasticity, many authors worked on the 2D application of the XFEM formulation for the analysis of cracks that constitutes a large part of industrial needs [11–15].

Feulvarch *et al.* [16] recently proposed a first XFEM formulation capable of overcoming the volumetric locking phenomenon due to von Mises plastic incompressibility in 3D. In this way, it is now possible to study the impact of plasticity on the fatigue propagation of cracks in 3D without restriction on the hardening behavior. Moreover, it can be extended to thermo-mechanical problems by introducing thermal expansion. This formulation is here applied to analyze a valve structure submitted to cyclic thermo-mechanical loading. Because of the curved geometry of the component, the simulation is carried out by means of quadratic hexahedral elements. The objective is to analyze the propagation of a crack in mode I. Compared to elastic behavior, plasticity introduces added variables into the history of propagation such as the plastic strain. Therefore, the simulation requires the treating of all the cycles, and the computing time can then increase.

In order to overcome such an issue, a computation strategy is developed in this paper by considering that the main impact of plasticity occurs during loading and focuses near the crack front. This way, unloading does not need to be considered and it is not necessary to simulate all the cycles. According to the deformation plasticity theory, the conventional $J$-integral can then be used without computing the plastic strain gradient that can be difficult to obtain inside the XFEM elements because of the high number of integration points.

The mixed XFEM formulation is developed in the first part of this paper by including thermal expansion. The strategy proposed to reduce the computing time is detailed in the second part. The propagation is assumed to be driven by Paris' law. The last part is dedicated to the simulation of crack propagation inside a valve structure submitted to cyclic thermo-mechanical loading. A comparison is made between an elastic computation and the elasto-plastic strategy proposed. This application clearly shows the influence of plasticity on the propagation path in the XFEM framework, which avoids remeshing difficulties.

## 2 XFEM formulation

### 2.1 Weak formulation

Under small strain assumption, the Cauchy stress tensor $\boldsymbol{\sigma}$ depends linearly on the elastic strain tensor $\boldsymbol{\epsilon}^e$:

$$\boldsymbol{\sigma} = 2\,\mu\,\boldsymbol{\epsilon}^e + \lambda\, tr\,(\boldsymbol{\epsilon}^e)\,\mathbf{I} \tag{1}$$

where $\mu$ and $\lambda$ denote the Lame's coefficients; $\mathbf{I}$ is the unit $2^{nd}$ order tensor.

As most of classical elasto-plastic models, the additive decomposition is applied to the strain tensor $\boldsymbol{\epsilon}\,(\mathbf{u})$:

$$\boldsymbol{\epsilon}\,(\mathbf{u}) = \frac{1}{2}\,\left(\boldsymbol{\nabla}\mathbf{u} + (\boldsymbol{\nabla}\mathbf{u})^T\right) = \boldsymbol{\epsilon}^e + \boldsymbol{\epsilon}^{th} + \boldsymbol{\epsilon}^p \tag{2}$$

where $\boldsymbol{\epsilon}^{th}$ and $\boldsymbol{\epsilon}^p$ are respectively the thermal and plastic strain tensors; $\mathbf{u}$ denotes the displacement field.

Considering the von Mises yield criterion, the volumetric strain $\boldsymbol{\nabla}\cdot\mathbf{u}$ is purely thermo-elastic. Thus, the stress balance can be written as follows:

$$\boldsymbol{\nabla}\cdot(2\,\mu\,\boldsymbol{\epsilon}^e) + \boldsymbol{\nabla}q = \mathbf{0} \quad \text{in } \Omega \tag{3}$$

$$\boldsymbol{\nabla}\cdot\mathbf{u} - \frac{1}{\lambda}\,q = 3\,\alpha\,(\theta-\theta_0) \quad \text{in } \Omega \tag{4}$$

$$\boldsymbol{\sigma}\,.\mathbf{n} = \mathbf{T}^{(p)} \quad \text{on } \Gamma_T \tag{5}$$

$$\mathbf{u} = \mathbf{u}^{(p)} \quad \text{on } \Gamma_u \tag{6}$$

where $q$ is proportional to the mean stress $p$ as $q = \frac{3\,\lambda}{2\,\mu+3\,\lambda}p$; $\mathbf{n}$ is the unit outward normal vector to the boundary $\partial\Omega$ $(= \Gamma_T \cup \Gamma_u)$ of the domain $\Omega$ corresponding to the studied volume; $\alpha$ is the linear thermal expansion coefficient; $\theta$ and $\theta_0$ are respectively the temperature and the initial reference temperature; $\mathbf{T}^{(p)}$ and $\mathbf{u}^{(p)}$ are the imposed stress vector and displacement.

Accounting for homogeneous Dirichlet boundary conditions for more convenience (see e.g. [17]), the weak formulation can be written as follows:

Find functions $(\mathbf{u}, q) \in U \times Q$ such that for all functions $(\boldsymbol{\delta}\mathbf{u}, \delta q) \in U \times Q$,

$$\int_\Omega 2\mu\boldsymbol{\epsilon}^e : \boldsymbol{\delta\epsilon}\,dv + \int_\Omega q\,\boldsymbol{\nabla}\cdot\boldsymbol{\delta}\mathbf{u}\,dv = \int_{\Gamma_T} \mathbf{T}^{(p)}\,\boldsymbol{\delta}\mathbf{u}\,ds$$

$$\int_\Omega \delta q\,\boldsymbol{\nabla}\cdot\mathbf{u}\,dv - \int_\Omega \frac{1}{\lambda}\,\delta q\,q\,dv = \int_\Omega \delta q\,\left(3\,\alpha\,(\theta-\theta_0)\right)\,dv \tag{7}$$

with

$$U = \left\{\mathbf{u} \in H^1(\Omega)\,|\;\mathbf{u} = 0 \text{ on } \Gamma_u\right\} \quad \text{and} \quad Q = L^2(\Omega)$$

### 2.2 Spatial discretization

By considering hexahedral quadratic finite elements, the XFEM approximations of $\mathbf{u}$ and $q$ are of the following form

$$\mathbf{u}^h = \sum_{i\in\mathcal{M}} N_i\,\mathbf{u}_i^{(\mathcal{M})} + \sum_{i\in\mathcal{H}} N_i^{lin}\,H\,\mathbf{u}_i^{(\mathcal{H})} + \sum_{i\in\mathcal{K}}\sum_{j=1}^{4} N_i^{lin}\,F_j^{(u)}\,\mathbf{u}_{ij}^{(\mathcal{K})} \tag{8}$$

$$q^h = \sum_{i\in\mathcal{M}} N_i\,q_i^{(\mathcal{M})} + \sum_{i\in\mathcal{H}} N_i^{lin}\,H\,q_i^{(\mathcal{H})} + \sum_{i\in\mathcal{K}}\sum_{j=1}^{2} N_i^{lin}\,F_j^{(q)}\,q_{ij}^{(\mathcal{K})} \tag{9}$$

where $\mathbf{u}_i^{(\mathcal{M})}$, $\mathbf{u}_i^{(\mathcal{H})}$, $\mathbf{u}_{ij}^{(\mathcal{K})}$, $q_i^{(\mathcal{M})}$, $q_i^{(\mathcal{H})}$ and $q_{ij}^{(\mathcal{K})}$ denote the unknowns at the node numbered $i$; $H$ and $F_j^{(\cdot)}$ are the jump and tip enrichment functions. $N_i$ corresponds to the shape functions associated to the quadratic continuous approximation. $N_i^{lin}$ denotes the linear finite element shape functions that construct the partition of unity as recommended by Stazi *et al.* [18]. Following Galerkin's standard approach, the functions $\boldsymbol{\delta}\mathbf{u}^h$ and $\delta q^h$ are taken of the same form.

By describing the geometry of the crack with the normal level set $\phi$ and the tangent level set $\psi$ (see [19]), the Heaviside function $H$ is defined as follows:

$$H = \begin{cases} 1 & \text{if } \phi \geq 0 \\ -1 & \text{otherwise} \end{cases} \tag{10}$$

$F_j^{(\cdot)}$ denotes the crack tip enrichment functions near the crack tip [20] respectively for the $\mathbf{u}^h$ and $q^h$:

$$\boldsymbol{F}^{(u)} = \left\{ \sqrt{r}\,\sin\left(\frac{\theta}{2}\right); \sqrt{r}\,\cos\left(\frac{\theta}{2}\right); \sqrt{r}\,\sin\left(\frac{\theta}{2}\right)\sin(\theta); \sqrt{r}\,\cos\left(\frac{\theta}{2}\right)\sin(\theta) \right\} \tag{11}$$

$$\boldsymbol{F}^{(q)} = \left\{ \frac{1}{\sqrt{r}}\,\cos\left(\frac{\theta}{2}\right); \frac{1}{\sqrt{r}}\,\sin\left(\frac{\theta}{2}\right) \right\} \tag{12}$$

with $r = \sqrt{\phi^2+\psi^2}$ and $\theta = \arctan\frac{\phi}{\psi}$.

The functions $\boldsymbol{F}^{(u)}$ and $\boldsymbol{F}^{(q)}$ have already been used by Legrain *et al.* [21] in nearly incompressible elasticity. The authors considered 2 different approximations for the displacement and the pressure in order to satisfy the LBB condition [22,23] which is not required in this paper because of the regularization presented in the next section.

One can note that it is possible to consider a shifted version of the enrichment functions [24]. This approach has the benefit to preserve the Kronecker delta property but it leads to a non-conforming approximation [25]. A procedure for the local near-orthogonalization of enrichment functions can also be applied for improving the conditioning of the resulting matrices [26]. As far as the convergence rate is concerned, it could be optimized by means of the numerical determination of enrichment functions [27].

In Eq. (11) and (12), the set $\mathcal{M}$ contains all the mesh nodes. $\mathcal{H}$ is the subset of nodes whose support is cut into two parts by the crack. By considering a topological enrichment, $\mathcal{K}$ is composed of the node subset whose support contains the crack tip as used in [8][28]. It is to be noticed that $\mathcal{H}$ and $\mathcal{K}$ are only composed of nodes associated with the linear approximation. Feulvarch *et al.* [16] showed that this approach has the capability of avoiding the volumetric locking problem for von Mises elasto-plasticity.

### 2.3 Regularization and numerical integration

Because of plastic incompressibility, the solution can exhibit spurious oscillations which need to be addressed. By considering the regularization technique proposed by Feulvarch *et al.* [29], the thermo-elasto-plastic problem is solved in an incremental way at each time step $t + \Delta t$:

$$\forall\, \boldsymbol{\delta}\mathbf{u}^h, \int_{\Omega^h} 2\mu \boldsymbol{\epsilon}^e_{t+\Delta t} : \boldsymbol{\delta}\boldsymbol{\epsilon}^h \, dv + \int_{\Omega^h} q^h_{t+\Delta t} \, \boldsymbol{\nabla} \cdot \boldsymbol{\delta}\mathbf{u}^h \, dv - \int_{\Gamma^h_T} \mathbf{T}^{(p)}_{t+\Delta t} \, \boldsymbol{\delta}\mathbf{u}^h \, ds = 0 \tag{13}$$

$$\forall\, \delta q^h, \int_{\Omega^h} \delta q^h \boldsymbol{\nabla} \cdot \boldsymbol{\Delta}\mathbf{u}^h \, dv - \int_{\Omega^h} \frac{1}{\lambda} \, \delta q^h \, \Delta q^h \, dv - \int_{\Omega^h} \boldsymbol{\nabla}\delta q^h \cdot \mathbf{S} \cdot \boldsymbol{\nabla}\Delta q^h \, dv$$

$$- \int_{\Omega^h} \delta q^h \, 3\,\alpha \, \Delta\theta \, dv = 0 \tag{14}$$

where $\Delta\theta$, $\boldsymbol{\Delta}\mathbf{u}^h$ and $\Delta q^h$ denote respectively the increments of $\theta$, $\mathbf{u}^h$ and $q^h$ between $t$ and $t + \Delta t$. $\mathbf{S}$ is a regularization tensor defined as follows:

$$\mathbf{S} = \mathbb{1}_0 \left( \Sigma_{i=1}^{N^e} \int_{\Omega^h} \mathbb{1}_0 \left( \Delta\epsilon^p \right) \, N_i \, \mathrm{d}V \right) \, \lambda(h) \, \overline{\mathbf{v}}^h \otimes \overline{\mathbf{v}}^h \, \Delta t \tag{15}$$

with

$$\lambda(h) = \frac{1}{2 \left( \overline{\mathbf{v}}^h \right)^2} \sqrt{\sum_{q=1}^{3} \left( h_q \, \overline{\mathbf{v}}^h . \mathbf{x}_q \right)^2}$$

$h_q$ is the length of a finite element in the direction $\mathbf{x}_q$ (see [30]); $N^e$ is the number of nodes of the element $e$; $\Delta\epsilon^p$ is the equivalent plastic strain increment; $\overline{\mathbf{v}}^h$ is the average velocity in the element $e$; $\mathbb{1}_0$ is an indicator function defined as follows:

$$\mathbb{1}_0 \left( x \right) \equiv \begin{cases} 1 & \text{if } x = 0, \\ 0 & \text{if } x \neq 0. \end{cases}$$

The indicator $\mathbb{1}_0$ allows selecting the finite elements to be stabilized. These are the elements presenting an increment of plastic strain which are embedded in a nearly incompressible plastic zone.

For the numerical integration of Eq. (13), each enriched hexahedral quadratic element is partitioned into a given number of tetrahedrons according to the sub-cell technique proposed by Loehnert *et al.* [31]. Each sub-tetrahedron contains 15 integration points if an asymptotic term needs to be calculated and only 1 point otherwise. The number of integration points can reach respectively 600 and 100 for the elements having nodes belonging to $\mathcal{K}$ and $\mathcal{H}$ depending on the way the crack crosses the elements. At each integration point, $\boldsymbol{\sigma}$ is computed by means of the radial return algorithm according to the associated theory of plasticity. By this way, $2\mu\,\boldsymbol{\epsilon}^e$ in Eq. $(13)_1$ is obtained as follows:

$$2\mu\,\boldsymbol{\epsilon}^e = \boldsymbol{\sigma} - \frac{\lambda}{3\lambda + 2\mu}\,tr\left(\boldsymbol{\sigma}\right)\,\mathbf{I} \tag{16}$$

## 3 Propagation computation strategy

### 3.1 Modeling strategy

According to the deformation plasticity theory, Rice [32] provided the basis for extending the fracture mechanics methodology well beyond the validity limits of LEFM. Indeed, the conventional $J$-integral can be applied by idealizing elasto-plastic deformation as nonlinear elastic. This theory is irrelevant for non-proportional loadings. Unfortunately, this can occur during unloading for elasto-plastic materials at each fatigue cycle. Therefore, it is not possible to use the conventional $J$-integral in this case. An improved version has been proposed by Simha *et al.* [33] to overcome this difficulty. It is very useful to characterize the crack growth rate in low-cycle fatigue [34–37].

In this paper, the plastic zone is growing around the crack front. This is not a case of extended plasticity through the whole structure. Thus, the increment of the stress intensity factor denoted $\Delta K_{eq}$ can be used to estimate the crack extension by means of Paris' law. The computation strategy proposed consists of applying the thermo-mechanical loading to the mesh free of plastic strain at each fatigue propagation step. This approach is of great interest because:

- it avoids the treatment of the nonlinear contact problem involved by the closing phenomenon during unloading;
- the conventional $J$-integral can be used in the context of the deformation plasticity theory for the evaluation of $K_{eq}$;
- it is not necessary to know the thorough history of plasticity which requires simulating all the fatigue cycles;
- the spatial derivative of the plastic strain does not need to be computed.

The mechanical history is taken into account by means of the evolution of the crack front geometry and the distribution of $K_{eq}$ at each propagation step along the crack front. The plasticity is assumed to have an influence on $K_{eq}$ only by means of its growth around the crack front during loading.

As far as XFEM modeling is concerned, the computation of the spatial derivative of the plastic strain would have been very difficult if it had been necessary because of the high number of integration points and the evolution of the XFEM enrichment functions.

### 3.2 Propagation computation

Considering propagation in mode I, the propagation computation consists first in evaluating the $J$-integral that can be expressed in the following volume integral form in the case of a constant value of $\alpha$:

$$J = -\int_V \left(P_{ij}\, w_{i,j} + w_i\, \sigma_{kl}\, \epsilon^{th}_{kl,\theta}\, \theta_{,i}\right)\, dV \tag{17}$$

where $P_{ij} = \frac{1}{2}\boldsymbol{\sigma} : \boldsymbol{\epsilon}\, \delta_{ij} - \sigma_{mj}\, u_{m,j}$ denotes the Eshelby's energy momentum tensor [38]; $V$ is the integration volume around the crack front; $\mathbf{w}$ is the perturbation field. It is to be noted that the crack faces are traction free in this work. The method proposed by Rajaram *et al.* [39] initially proposed for FEM calculations has been chosen and developed in the XFEM framework because of its robustness and its low sensibility to spatial discretization. Once $J$ is computed at different point of analysis located on the crack front (defined by $\phi$=0 and $\psi$=0), the stress intensity factor $K_{eq}$ is evaluated under the plane strain assumption:

$$K_{eq} = \sqrt{\frac{E\, J}{1-\nu^2}} \tag{18}$$

where $E$ and $\nu$ denote the Young's modulus and the Poisson's coefficient respectively. Then, the crack advance $\Delta a$ is evaluated by means of the Paris law:

$$\frac{\Delta a}{\Delta N} = C\, (\Delta K_{eq})^m \tag{19}$$

where $C$ and $m$ are material coefficients; $\Delta K_{eq}$ is the variation of $K_{eq}$ on the duration $\Delta N$. It must be noted that such a law is not appropriate for elasto-plastic materials but it is applied here to illustrate the impact of plasticity by comparing elastic and elasto-plastic simulations.

From the simulation point of view, $\Delta N$ is first computed at the point of analysis where $\Delta K_{eq}$ is maximal. By prescribing the value $\Delta a^{max}$ at this location, the crack advance is then evaluated at the other points of analysis. This controls the evolution of the propagation with a constant maximal extension length. A second order B-Spline smoothing method [40] is used for modeling the evolution of $\Delta K_{eq}$ along the crack front. This ensures a smooth transformation of the crack front during propagation. Assuming propagation in the mode I, the evolution of the crack front is simulated by updating the level set $\psi$ according to $\Delta a$ whereas $\phi$ stays unchanged. A B-spline interpolation is used to represent the crack front and compute the new position of the points of analysis by means of an orthogonal projection.

## 4 Propagation analysis in a valve structure

This application concerns a valve structure of 400mm length shown in Fig. 1(a). The internal diameter is equal to 140mm on both sides. A circumferential crack is inserted into the inner skin as shown in Fig. 1(b). Fig. 1(c) shows half of the crack because the other part is inserted in the plotted part of the 3D mesh. The crack is located in the fillet underneath the gasket seat and it has an orientation angle of $45^o$ degrees with the axis of the structure. It is elliptical, 7 mm deep, and 40 mm wide and it lies on a cone-type surface. The mesh size denoted $h$ decreases in the crack area, with hexahedrons of about 1.25mm side. All the simulations have been performed using the computer code Systus® [41].

The valve structure is submitted to thermo-mechanical transient loading representative of an industrial situation. The initial temperature $\theta_0$ of the structure is taken equal to $325^o$C. A cooling stage occurs because of the fluid flow inside the valve. This is simulated by considering a heat exchange coefficient of $5.10^4$W.m$^{-2}$ on the internal surface associated with an internal temperature decreasing as indicated in Tab. 1. The thermal properties of the valve structure are constant and given in Tab. 2.

The cooling stage was computed one time on the structure without accounting the crack. Then, the computed thermal history was applied to the structure with the pressure prescribed on the internal surface and the bending moment applied along the z-axis (see Tab. 1). The temperature distribution is plotted in Fig. 2 at 100s corresponding to the end of the loading stage.

| Time (s) | Int. temperature ($^o$C) | Int. pressure (MPa) | Bending moment ($10^4$N.m) |
|---|---|---|---|
| 0 | 325 | 0 | 0 |
| 20 | 272 | 16 | 0.4 |
| 100 | 60 | 16 | 2 |

**Table 1** Thermo-mechanical loading.

| Conductivity (W m$^{-1}$ $^o$C$^{-1}$) | Mass per unit volume (kg m$^{-3}$) | Heat capacity (J $^o$C$^{-1}$ kg$^{-1}$) |
|---|---|---|
| 15 | 7850 | 480 |

**Table 2** Thermal properties of the valve structure.

The mechanical boundary conditions allow only a radial dilatation of the clamped face. One can note that the bending moment along the z-direction is generated by means of the repartition of nodal forces. The internal pressure is applied with the associated closed end pressure. The elasto-plastic behavior considered here includes isotropic hardening with a hardening modulus of 4000 MPa. The yield stress $\sigma^y$, $E$ and $\nu$ are respectively equal to 246MPa, 200000

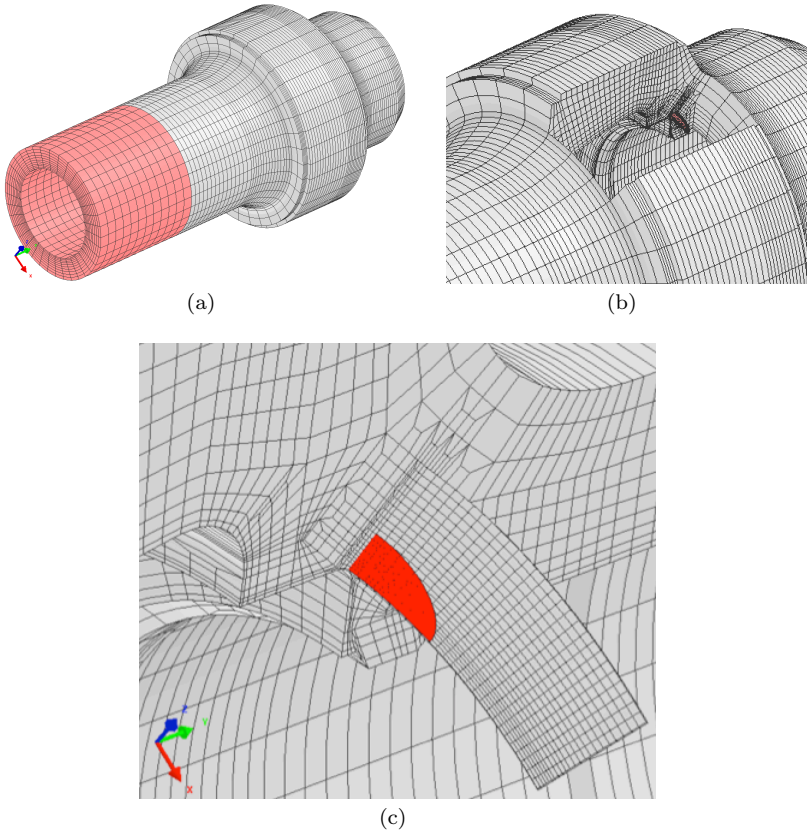

**Fig. 1** (a) - Global geometry of the valve structure (grey) with the zone for mechanical load application (red); (b) - Position of the crack in the fillet located underneath the gasket seat; (c) - XFEM discretization in the zone containing the crack with $h = 1.25mm$ (red).

MPa and 0.3. The value of the linear thermal expansion coefficient is constant: $16.10^{-6}\mathrm{K}^{-1}$.

A comparison of the distributions of the von Mises stress before propagation is shown on Fig. 3 between a FEM calculation carried out with a refined mesh of the crack and the XFEM simulation. One can note that the XFEM distribution is satisfactory even if the values are lower around the crack front because of the averaging step used for plotting in the enriched elements.

The evolution of the $J$ computed with XFEM along the crack front is plotted in Fig. 4 before propagation just after the first loading operation. A second refined mesh ($h = 0.7mm$) has been considered to show that the element size has no significant influence on the distribution of $J$. The plasticity reduces the values of $J$ especially on each side of the crack where it is more intense as shown in Fig. 3 by means of the von Mises stress. Compared to the elastic simulation, the propagation rate in elasto-plasticity is then lower on

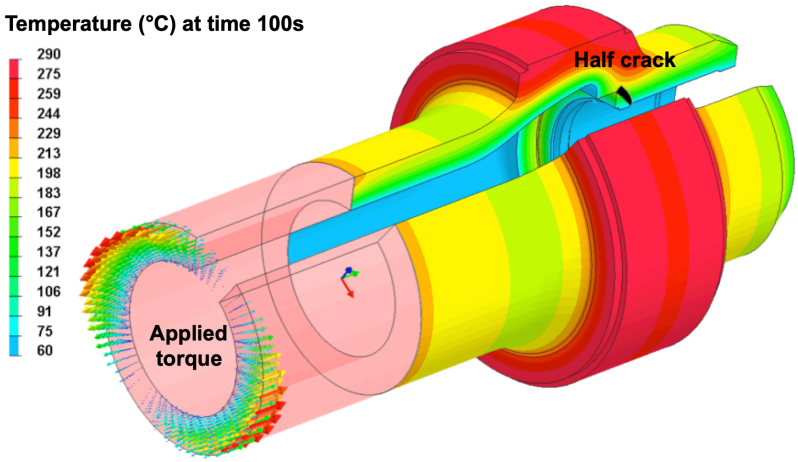


**Fig. 2** The Temperature field at time 100s; distribution of nodal forces (left of the figure) representing a bending moment along the z-axis.

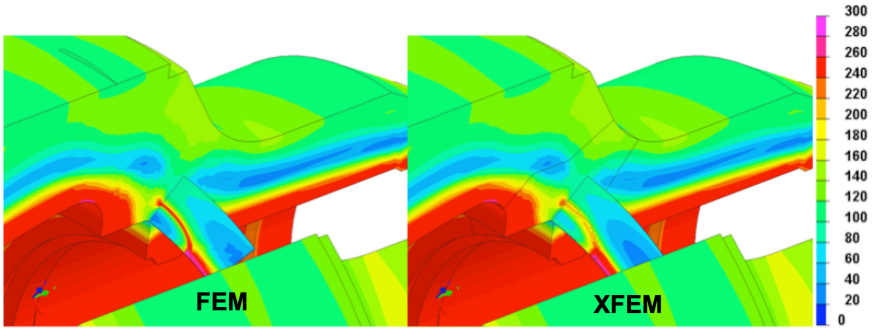


**Fig. 3** Distribution of the von Mises stress (MPa) at time 100s before starting the propagation simulation.

the ends of the crack front as shown on the half crack in Fig. 5 for the same number of cycles.

Under thermal-driven loading, strains are imposed and therefore, plasticity reduces the stress level but does not increase strains. This induces lowering of $J$. One can note that it is not necessary in the case of mechanical-driven loadings.

Fig 6 shows the evolution of all the crack fronts in elasto-plasticity. One can note that the crack has a quasi-symmetrical geometry even if mechanical loading is not symmetric because of the bending moment. It is important to note that the Paris law used in this paper is not appropriate for elasto-plastic materials but this application illustrates the capability of the numerical approach proposed to include the impact of plasticity on the fatigue propagation of a crack.

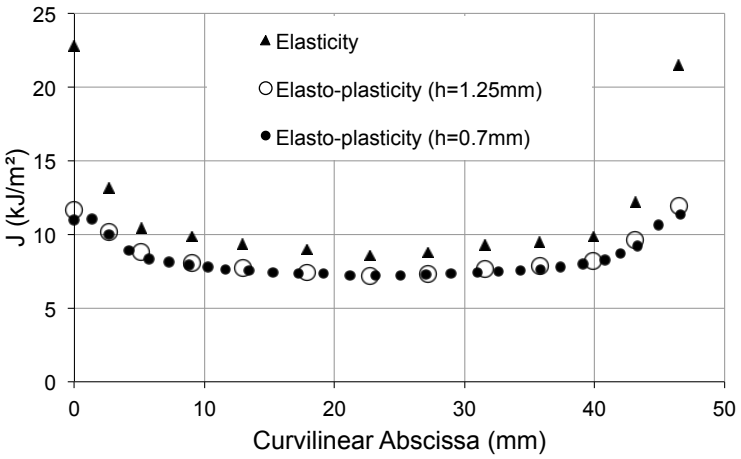


**Fig. 4** Evolution of $J$ along the crack front obtained with XFEM at time 100s before starting the propagation simulation.

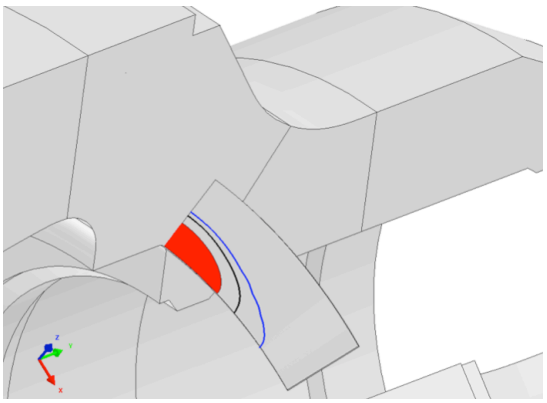

**Fig. 5** Comparison between the geometries of the crack front obtained with XFEM in elasticity (blue) and elasto-plasticity (black).

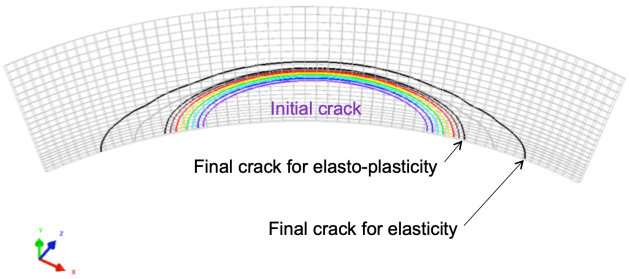


**Fig. 6** Evolution of the crack front obtained with XFEM in elasto-plasticity (in colors).

## 5 Conclusion

In this paper, a 3D XFEM strategy has been developed in order to simulate the planar propagation of a crack under cyclic thermo-mechanical loading. The first interest of such an approach is the use of XFEM permitting to avoid remeshing problems. The second originality is the use of an elasto-plastic behavior to simulate a propagation phenomenon in the XFEM framework in 3D. The third main characteristic is the calculation strategy which does not require computing all the elasto-plastic cycles and uses the conventional $J$-integral in the context of the deformation plasticity theory. Future work will focus on the study of more complex propagations not restricted to extension in mode I.

## References

1. Moes N., Dolbow J. and Belytschko T. (1999). A finite element method for crack growth without remeshing, International Journal for Numerical Methods in Engineering, 46, 131-150.
2. Sutula D., Kerfriden P., van Dam T., Bordas S.P.A., Minimum energy multiple crack propagation. Part II: Discrete Solution with XFEM, Eng. Fract. Mech. 191 (2018) 225-256.
3. Sukumar N., Moes N., Moran B., Belytschko T., Extended finite element method for three-dimensional crack modelling, Internat. J. Numer. Methods Engrg. 48 (2000) 1549-1570.
4. Moes N. , Gravouil A., Belytschko T., Non-planar 3D crack growth by the extended finite element and level sets-Part I: Mechanical model, Internat. J. Numer. Methods Engrg. 53 (11) (2002) 2549-2568.
5. Bordas S., Moran B., Enriched finite elements and level sets for damage tolerance assessment of complex structures, Eng. Fract. Mech. 73 (9) (2006) 1176-1201.
6. Sadeghirad A., Chopp D., Ren X., Fang E., Lua J., A novel hybrid approach for level set characterization and tracking of non-planar 3d cracks in the extended finite element method, Eng. Fract. Mech. 160 (2016) 114.
7. Jin Y., Gonzlez-Estrada O., Pierard O., Bordas S.P.A., Error-controlled adaptive extended finite element method for 3d linear elastic crack propagation, Comput. Methods Appl. Mech. Engrg. 318 (2017) 319348.
8. Feulvarch E., Fontaine M., Bergheau J.-M., XFEM investigation of a crack path in residual stresses resulting from quenching, Finite Elements in Analysis and Design 75 (2013) 62-70.
9. Bordas S., Rabczuk T., Zi G., Three-dimensional crack initiation, propagation, branching and junction in non-linear materials by an extended meshfree method without asymptotic enrichment, Engineering Fracture Mechanics 75 (2008) 943-960.
10. Penga X., Atroshchenkob E., Kerfridena P., Bordas S.P.A., Isogeometric boundary element methods for three dimensional static fracture and fatigue crack growth, Comput. Methods Appl. Mech. Engrg. 316 (2017) 151-185.
11. Elguedj T., A. Gravouil, A. Combescure, Appropriate extended functions for XFEM simulation of plastic fracture mechanics, Comput. Methods Appl. Mech. Eng. 195 (2006) 501515.
12. Kumar S., Singh I. V., Mishra B. K., XFEM simulation of stable crack growth using J-R curve under finite strain plasticity, Int J Mech Mater Des (2014) 10 :165-177.
13. Pandey V.B. , Singha I.V., Mishra B.K., Ahmad S., Venugopal Rao A., Kumar V., A new framework based on continuum damage mechanics and XFEM for high cycle fatigue crack growth simulations, Engineering Fracture Mechanics 206 (2019) 172-200.
14. Kumar S., Singh I.V., Mishra B.K., Sharma K., Khan I.A., A homogenized multigrid XFEM to predict the crack growth behavior of ductile material in the presence of microstructural defects, Engineering Fracture Mechanics 205 (2019) 577-602.

15. Shanga H. Y., Machadob R.D., Filho J.E.A., On the performance of GFEM with trigonometric enrichment in bidimensional dynamic elastoplastic modelling, European Journal of Mechanics / A Solids 73 (2019) 512-527.
16. Feulvarch E., Lacroix R., Deschanels H., A 3D locking-free XFEM formulation for the von Mises elasto-plastic analysis of cracks, Comput. Methods Appl. Mech. Engrg, 361, (2020), 112805.
17. Brezis, H., Functional analysis, Sobolev spaces and partial differential equations, Springer, 2011.
18. Stazi F. L., Budyn E., Chessa J., Belytschko T., An extended finite element method with higher-order elements for curved cracks, Computational Mechanics 31 (2003) 38-48, DOI 10.1007/s00466-002-0391-2.
19. Elguedj T., Gravouil A., Maigre H., An explicit dynamics extended finite element method. Part 1: Mass lumping for arbitrary enrichment functions, Comput. Methods Appl. Mech. Engrg. 198 (2009) 2297-2317.
20. Westergaard, H.M. (1939). Bearing pressures and cracks, J. Appl. Mech., 6, 49-53.
21. Legrain G., Moes N., Huerta A., Stability of incompressible formulations enriched with XFEM, Comput. Methods Appl. Mech. Engrg. 197 (2008) 1835-1849.
22. Babuška I., The finite element method with Lagrangien multipliers, Numer Math., vol. 20,pp. 179-192, 1973.
23. Brezzi F., On the existence, uniqueness and approximation of saddle-point problems arising from Lagrangian multipliers, RAIRO, Anal. Numer, R2, pp. 129-151, 1974.
24. Zi G., Belytschko T., New crack-tip elements for xfem and applications to cohesive cracks, Internat. J. Numer. Methods Engrg. 57 (15) (2003) 2221-2240.
25. Stapor P., Application of XFEM with shifted-basis approximation to computation of stress intensity factors, Archive of Mechanical Engineering, 10.2478/v10180-011-0028-0, (2012), Vol 58: 4, 447-483.
26. Agathos K., Bordas S.P.A., Chatzia E., Improving the conditioning of XFEM/GFEM for fracture mechanics problems through enrichment quasi-orthogonalization, Comput. Methods Appl. Mech. Engrg. 346 (2019) 1051-1073.
27. Menk A., Bordas S. P. A., Numerically determined enrichment functions for the extendednite element method and applications to bi-material anisotropicfracture and polycrystals, Int. J. Numer. Meth. Engng 2010; 83:805-828.
28. Tumbajoy-Spinel D.Y., Feulvarch E., Bergheau J.M., Kermouche G. (2013). 2D axisymmetric X-FEM modeling of the Hertzian cone crack system, *Comptes Rendus Mecanique*, Volume 341, Issues 910, (2013), Pages 715-725.
29. Feulvarch E., Roux J.-C., Bergheau J.-M., Gilles P., A stable P1/P1 finite element for finite strain von Mises elasto-plasticity, Comput. Methods Appl. Mech. Engrg. 324 (2017) 537-545.
30. A. N.Brooks, T. J.R.Hughes, Streamline upwind/Petrov-Galerkin formulations for convection dominated flows with particular emphasis on the incompressible Navier-Stokes equations, Computer Methods in Applied Mechanics and Engineering, Volume 32, Issues 1-3, September 1982, Pages 199-259.
31. Loehnert S., Mueller-Hoeppe D.S., Wriggers P., 3D corrected XFEM approach and extension to finite deformation theory, Internat. J. Numer. Methods Engrg. 86 (45) (2011) 431452.
32. Rice J.R., A Path Independent Integral and the Approximate Analysis of Strain Concentration by Notches and Cracks, J. Appl. Mech. Jun (1968), 35(2), 379-386.
33. Simha N.K., Fischer F.D., Shan G.X., Chen C.R., Kolednik O., J-integral and crack driving force in elastic-plastic materials, Journal of the Mechanics and Physics of Solids, 56, (2008), 2876-2895.
34. Fischer F.D., Simha N.K., Predan J., Schongrundner R., Kolednik O., On configurational forces at boundaries in fracture mechanics, International Journal of Fracture, 174, (2012), 61-74.
35. Kolednik O., Schongrundner R., Fischer F.D., A new view on J-integrals in elastic-plastic materials, International Journal of Fracture, 187, (2014), 77-107.
36. Ochensberger W., Kolednik O., A new basis for the application of the J-integral for cyclically loaded cracks in elastic-plastic materials, International Journal of Fracture, 189, (2014), 77-101.

37. Ochensberger W., Kolednik O., Physically appropriate characterization of fatigue crack propagation rate in elastic-plastic materials using the J-integral concept, International Journal of Fracture, 192, (2015), 25-45.
38. Eshelby JD, Energy relations and the energy-momentum tensor in continuum mechanics, In: Kanninen MF, Adler WF, Roseneld AR, Jaee RI, editors. Inelastic behavior of solids. New York: McGraw Hill, (1970).
39. Rajaram H., Socrate S., Parks D.M., Application of domain integral methods using tetrahedral elements to the determination of stress intensity factors, Engineering Fracture Mechanics, 66, (2000), 455-482.
40. Dierckx P., Curve and Surface Fitting with Splines, Oxford University Press, Oxford, (1993).
41. ESI Group, Users Manual, 2020.